Strathprints Institutional Repository

Modelling and Control of a Plastic Film Manufacturing Web Process

Sung-ho Hur, Reza Katebi, and Andrew Taylor

***Abstract*—This paper is concerned with the modelling of a plastic film manufacturing process and the development and implementation of a model-based Cross-Directional (CD) controller. The model is derived from first-principles and some empirical relationships. The final validated nonlinear model could provide a useful off-line platform for developing control and monitoring algorithms.**

A new controller is designed which has a similar structure to that of Internal Model Control (IMC) with the addition of an observer whose gain is designed to minimise process and model mis-match. The observer gain is obtained by solving a multi-objective optimisation problem through the application of a genetic algorithm. The controller is applied to the nonlinear model and simulation results are presented demonstrating improvements that can be achieved by the proposed controller over two existing CD controllers.

***Index Terms*—Plastic film manufacturing, web process, 2D control design and tuning, optimisation, and industrial control.**

I. Introduction

The first part of this paper reports on the development of a nonlinear model of a plastic film manufacturing process. The modelling of a large-scale process, such as the one concerned in this paper, can be time consuming and complex, and such a model is therefore still rare. However, when such a model becomes available, it can bring many advantages. For instance, most model-based control and monitoring algorithms require a state-space or transfer function model identified from the process. Assuming that the model is accurate, it can be used to simulate the process enabling shorter and more flexible process experiments leading to less wasted product. The model could also allow new and existing control and monitoring algorithms to be developed, tested, and compared to improve plant performance. By adding disturbances and faults, realistic scenarios where faults and disturbances are present can be simulated without the need for experiments on the real process. Moreover, the model would also allow for the design of the spatial characteristics, optimal position, and spacing of sensors and actuators [1].

As with other web forming processes, such as the papermaking and metal-rolling, plastic film extrusion employs arrays of actuators across a continuously moving web to control the Cross-Directional (CD) thickness profile of the finished product as measured by a scanning gauge downstream of the process. CD control has received a considerable attention in the academic community and there have been many papers published studying various CD controller designs [2]. The second part of this paper reports the development of a new model-based CD controller. The performance of this controller is assessed by application to the nonlinear model and comparing it with two other existing controllers. This model is used to simulate the plant throughout this paper.

The proposed controller design has a similar structure to that of the controller reported in [3] since both are modifications to Internal Model Control (IMC). The controller presented here requires the online solution of a quadratic programming problem to achieve optimal steady state performance subject to actuator and bending constraints. Model-based CD controllers require an accurate reference model and controller performance can be improved by minimising the effects of process-model mismatch and disturbances. Consequently, the proposed controller design employs an observer in place of the reference model in order to reduce the effect of process-model mismatch as well as disturbances.

A brief description of the plastic film manufacturing process is presented in Section II, and the development and validation of the nonlinear model are described in Section III. The CD controller is introduced in Section IV, and the performance of the proposed controller and comparison with existing ones are reported in Section V. Conclusion is drawn in Section VI.

II. Process Description

Fig. 1 depicts a process flow diagram of the film manufacturing process, which produces biaxially oriented polyethelene terephthalate (PET) and polyethelene naphthalate (PEN) films by stretching the film in the Cross-Direction (CD) and Machine-Direction (MD) [4]. In the preparation stage the virgin polymer is converted into pellets which are then melted via extrusion and fed into the die. The die releases a polymer melt curtain (1.0 - 2.0 m by 4.0 mm), which is drawn down and quenched on a casting drum to form a cast web or film. This film is conveyed along the surfaces of the casting drum, quench roll and slow-nip rolls and reaches the preheat rolls. The fast and slow nip rolls are speed controlled, and the speed difference between them stretches the film in the MD with stretch ratio of approximately 3 to 1. The purpose of the preheat rolls is to increase the temperature of the film above its glass transition temperature, and the cooling rolls cool down the film to strengthen the mechanical properties of the film formed during the stretching process.

The stenter oven comprises of four stages: pre-heat oven, sideways-draw, crystalliser, and cooling zone. The pre-heat

This work was supported by DuPont Teijin Films UK Ltd, UK EPSRC Industrial CASE Award, and UK EPSRC Platform Grant (GR/R04683/01).

S. Hur and R. Katebi are with the Department of Electronic and Electrical Engineering, University of Strathclyde, U.K (e-mail: sunghur@ieee.org).

A. Taylor is with DuPont Teijin Films UK Ltd.

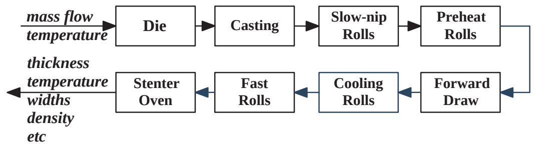

Fig. 1. Process flow diagram

oven raises the film temperature such that it can be stretched more easily. During the second stage of the stenter oven, the edges of the film are clipped and led along diverging rails causing the film to stretch in the CD. Typically the width of the film is increased in the sideways draw to approximately 3 times its original width. The stretched film structure is then heat set in the crystalliser and cooling zone by first heating and then quickly cooling the film. The finished film, now roughly a ninth of the cast film thickness, is spooled onto a roll and transported away for processing.

The CD thickness profile of the film formed on the casting drum is varied in order to control the CD thickness profile of the finished film. This is achieved by adjusting the CD thickness profile of the mass flow rate discharged through the die-lip gap using actuators that locally heat the polymer to decrease the melt viscosity and thus increases the mass flow rate, or vice versa.

III. The Nonlinear Model

To track changes in the thickness profile, it requires tracking changes in temperature, velocity, and widths of the film at positions along the MD and CD of film path. For modelling purposes the process is decomposed into a series of unit operations as depicted in Fig. 1. Within each of these unit operations the film path is meshed in the MD (x-direction) and CD (y-direction) using a uniform rectangular mesh (see Fig. 3). Modules (or sub-models) for mass-transfer, heat-transfer and deformation are then formulated for each unit operation and fitted to the mesh.

In the next two sub-sections, the mass and heat transfer modules, which are common for all unit operations, are presented. These are followed by the descriptions of how these modules can be applied to each of the unit operations.

A. Mass transfer model

To capture the dynamic variation in the film thickness, the mass per unit area of the film is defined as basis weight (W in kg/m^2). The thickness can then be defined as basis weight per density of the film. Tracking the basis weight variation along the MD and CD of the film will then be equivalent to tracking the thickness variation. Assuming that the film travels at velocity $v_m(t)$ (m/s) in the MD only and Δx and Δy denote the length and width of each mesh section (see Fig. 3), the basis weight at position $(i\Delta x, j\Delta y)$ of the film can be described as

$$\frac{\partial W_{i,j}(t)}{\partial t} = v_m(t)\frac{W_{i-1,j}(t) - W_{i,j}(t)}{\Delta x} \tag{1}$$

The above equation describes the mass flow in each of the rectangular mesh sections along the film path. The velocity is assumed to be constant for a given Δx.

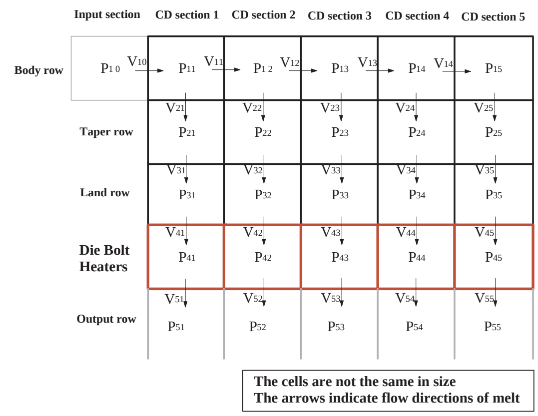

Fig. 2. 2-D explanatory view of the die component of the film manufacturing process

B. Heat transfer model

Due to the relatively high transport velocity of the film, it is assumed that conductive heat transfer within the film can be neglected. The temperature, $T_{i,j}(t)$, at position $(i\Delta x, j\Delta y)$ can therefore be modelled using the following convective heat transfer equation,

$$\frac{\partial T_{i,j}(t)}{\partial t} = v_m(t)\frac{T_{i-1,j}(t) - T_{i,j}(t)}{\Delta x} + \frac{Q(t)}{c_f W_{i,j}(t)\Delta x\Delta y} \tag{2}$$

where c_f and $Q(t)$ denote the specific heat of the film $(J/kg/K)$ and the heat added or removed from the film (J/s), respectively.

The top and bottom surfaces of the film are either in contact with a roll surface or exposed to air. For the surface in contact with a roll surface, the following heat transfer equation is used:

$$Q_c(t) = \Delta x\Delta y h_c(T_c(t) - T_{i,j}(t)) \tag{3}$$

where h_c and $T_c(t)$ respectively denote the heat transfer coefficient $(J/s/m^2/K)$ and the temperature of the cooling/heating medium, such as air or water, inside the roller. For the film surface exposed to air, heat transfer by radiation or convection is considered, leading to the following heat transfer equation:

$$\begin{aligned} Q_a(t) &= \Delta x\Delta y\left(h_a(T_a(t) - T_{i,j}(t)\right) \\ &\quad + \Delta x\Delta y\left(\sigma\epsilon(T_a(t)^4 - T_{i,j}(t)^4)\right) \end{aligned} \tag{4}$$

where σ denotes Stefan Boltzmann's constant (J/s/m^2/K^4) and ϵ the emissivity. Heat transfer coefficients, h_c and h_a, are dependent on temperature and therefore vary throughout the process.

Heat transfer within the stenter is mainly carried out by blowing hot or cold air onto the surfaces of the film, in which case only the first term of (4) is employed.

C. Die

The process starts with polymer melt that is fed into the die through a circular pipe connected to one side of the die. Due to the mechanical design of the die, the melt flow is distributed almost evenly along the width of the die and subsequently discharged through the die gap onto the casting drum. Die bolt heaters mounted across the width of the die are used by the CD control system to manipulate the melt flow. The actuator outputs for these heaters are provided by the CD control system based on the CD thickness profile of the finished product.

For modelling purposes, the die is considered as being comprised of interconnected pipes which construct a flow mesh as shown in Fig. 2 – the figure assumes that the die is divided into 5 sections for brevity. The flow is thus assumed to travel horizontally in the die body row and vertically through the taper and land rows as depicted in the figure. The horizontal and vertical flows are respectively described by Poiseuille's law for laminar flow of viscous fluid as follows [5]:

$$P_{i+1,j} - P_{i,j} = \frac{3\mu L_{i,j}}{\pi R_{i,j}^4} V_{i+1,j} \tag{5}$$

and

$$P_{i,j+1} - P_{i,j} = \frac{3\mu L_{i,j}}{\pi R_{i,j}^4} V_{i,j+1} \tag{6}$$

where μ is the viscosity of the polymer melt, $L_{i,j}$ and $R_{i,j}$ are the appropriate pipe length and radius of each CD section, $P_{i,j}$ is the pressure in section (i, j), and $V_{i,j}$ is the volumetric flow in section (i, j).

To empirically model the effect of the die bolt heaters the following pressure flow relation is used:

$$P_{i+1,j} - P_{i,j} = k_j V_{i,j} \tag{7}$$

where the coefficient k_j is a viscosity factor given by

$$k_j = \beta_1 x_j + \sum_{n=1}^{N_s} (\beta_{n+1} x_{j-n} + \beta_{n+1} x_{j+n}) \tag{8}$$

where β is a vector of coefficients derived from the actuator interaction, x is a vector of die bolt heater settings, and N_s is a constant determined by the size of the actuator interaction. The form of (8) is derived from the observation that a particular die bolt heater affects the flow rate of not only the corresponding region of the film but also the neighbouring region.

By combining the above equations with appropriately selected continuity equations the flow conditions within the die can be computed by solving a linear system of equations.

D. Casting Drum

When the polymer melt is released through the die-lip gap onto the surface of the casting drum, a thick film is formed. The thickness of this film is determined by the mass flow rate leaving the die-lip gap and the speed of the casting drum. In order to compute the mass per unit area deposited onto the casting drum at a position $j\Delta y$ along the width of the casting drum, the following formula is used:

$$W_j(t) = \frac{\dot{m}_j(t)}{v_m(t) \Delta y_j(v_m(t), T_j(t))} \tag{9}$$

where $\dot{m}_j(t)$ denotes the mass flow rate (kg/s) released through the die-lip gap at position $j\Delta y$, $v_m(t)$ is the velocity of the casting drum, and $\Delta y_j(v_m(t), T_j(t))$ refers to a scalar function that returns a correction factor to compensate for the fact that the film shrinks in the width direction near the edges – this phenomenon is known as neck-in. The function $\Delta y_j(v_m(t), T_j(t))$ may be obtained by solving a computational fluid dynamics problem for different casting drum velocities and discharge temperatures.

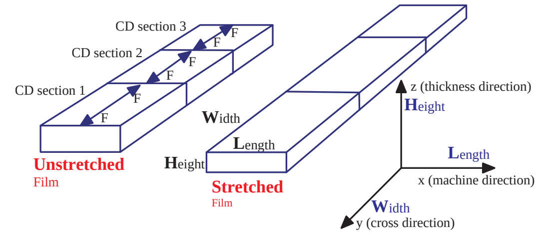

Fig. 3. Sideways Draw

The heat transfer and mass transfer associated with the casting drum process is modelled using the heat and mass transfer models presented in Sections III-A and III-B.

E. Pre-heating, Slow-nip, Fast-nip, and Cooling Rolls

These unit operations are all modelled using the previously presented mass and heat transfer models.

F. Forward draw

The film is stretched in the MD due to the speed difference between the slow and fast-nip rolls. The mass flow rate leaving the slow-nip rolls at position $j\Delta y$ can be computed by

$$\dot{m}_j(t) = W_j(t) v_s(t) \Delta y \tag{10}$$

where $v_s(t)$ denotes the velocity of slow nip rolls. Due to the law of mass conservation, the mass flow rate at the fast nip rolls must be the same, giving the following relation to compute the mass of the stretched film, $\tilde{W}_j(t)$,

$$\tilde{W}_j(t) = \frac{W_j(t) \Delta y v_s(t)}{v_f(t) \Delta y_j(v_f(t)/v_s(t), T_j(t))} \tag{11}$$

where $v_f(t)$ denotes the velocity of fast-nip rolls and $\Delta y_j(v_f(t)/v_s(t), T_j(t))$ refers to a scalar nonlinear function that compensates for the neck-in phenomenon.

G. Stenter Oven

The stenter oven is comprised of pre-heat oven, sideways-draw, crystalliser, and cooling zone. Apart from sideways-draw, these unit operations can be modelled using the generic models for heat and mass transfer presented in Section III-B.

The behaviour of the film during the sideways-draw depends on factors such as speed, thickness, and temperature. To develop a mathematical model of the sideways-draw, a CD strip of the film is considered as shown in Fig. 3. For brevity, the film strip in Fig. 3 is divided into three CD sections. This figure illustrates the effect of stretching. Note that the unstretched film is divided into sections with uniform widths, but different heights. The stretched film on the other hand exhibits non-uniform section widths and heights. Since the same stretching force acts on each section of the film, thinner sections are more prone to stretch than thicker sections.

In order to develop a mathematical model of the sideways draw, the concept of strain (stretched length) will be introduced. Strain can be defined as

$$\varepsilon_j = \frac{\tilde{w}_j - w_j}{w_j} \tag{12}$$

where $\tilde{w}_j$ denotes the stretched width of the film in section j and w_j is the un-stretched width of the film in section j. Using the equation above, the stretched width can be written as

$$\tilde{w}_j = w_j(\varepsilon_j + 1) \tag{13}$$

Since the un-stretched width of each section of the film is uniform, the above expression can be written as

$$\tilde{w}_j = \frac{w}{n}(\varepsilon_j + 1) \tag{14}$$

where w is the total un-stretched width of the film such that

$$w = w_1 + w_2 + \cdots + w_n \tag{15}$$

and n denotes the number of sections. Substituting (15) in (14) gives

$$\tilde{w} = \frac{w}{n}(\varepsilon_1 + 1) + \frac{w}{n}(\varepsilon_2 + 1) + \cdots + \frac{w}{n}(\varepsilon_n + 1)$$

The stress (stretch force) acting on each section of the film can be computed using

$$\sigma_j = \frac{F}{A_j} \tag{16}$$

where F is the equal force acting on each section and A_j is the cross sectional area of the j^{th} section.

The stress acting on the j^{th} section can be related to the strain of the j^{th} section by a stress-strain relationship [4]. The stress-strain relationship adopted in this instance is nonlinear function that depends on stretch temperature, average strain rate, and velocity as follows:

$$\sigma_j = f(\varepsilon_j, T_j, v_m) \tag{17}$$

which is an empirical model based on laboratory experiments.

Combining (16) and (17), a system of nonlinear equations can be obtained and solved for F and ε_j.

The full details of the model are presented in [6].

IV. Cross Directional Control

There are two approaches [3] to cross-directional control design. The first approach uses robust control design methods to provide a good degree of stability and performance robustness and the constraints are dealt with limited anti-windup. The second approach uses model based predictive control methods, which directly includes the constraints, and hence provide a better steady-state response. The proposed method belongs to the first approach, but an optimisation problem is proposed and solved online to improve the steady state response.

A model-based controller requires a reference model. One advantage of the controller proposed here is that there is no need to separate the dynamic component from the spatial component unlike the controller design reported in [3]. The derivation of a model in such a form requires a system identification process similar to the one described in [2].

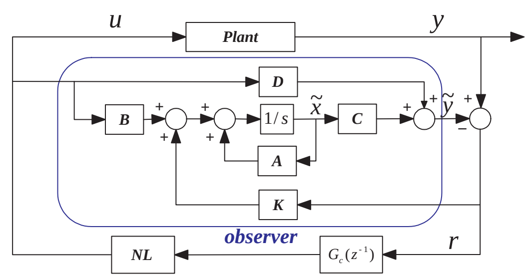

Fig. 4. Proposed controller

Instead, the proposed controller design utilises the System Identification Toolbox™7 in Matlab®to derive a linear model. This state space model is used to construct an observer which is then employed as the reference model. The observer can be designed to minimise the effects of process-model mismatch and disturbances, thereby improving the controller performance.

The full details of the identified linear models can be found in [7].

A. Observer Design

The mathematical description of the observer is as follows:

$$\begin{aligned}\dot{\tilde{\mathbf{x}}}(t) &= \mathbf{A}\tilde{\mathbf{x}}(t) + \mathbf{B}\mathbf{u}(t) + \mathbf{K}(\mathbf{y}(t) - \tilde{\mathbf{y}}(t)) \\ \tilde{\mathbf{y}}(t) &= \mathbf{C}\tilde{\mathbf{x}}(t) + \mathbf{D}\mathbf{u}(t)\end{aligned} \tag{18}$$

where $\mathbf{y}(t) \in \mathbb{R}^n$ and $\tilde{\mathbf{y}}(t) \in \mathbb{R}^n$ denote the plant measurements and model estimates, respectively, and $\mathbf{u}(t) \in \mathbb{R}^m$ represents the control action – note that $\mathbf{A}$ is square. The term involving the observer gain $\mathbf{K}$ should correct the observer estimate continuously such that $\tilde{\mathbf{y}}(t)$ follows $\mathbf{y}(t)$ more closely. This implies that the effects of process-model mismatch and disturbances can be reduced by optimising $\mathbf{K}$. Derivation of an optimal gain $\mathbf{K}$ is summarised in this section. $\mathbf{G}_c(z^{-1})$ and the nonlinear element (NL) in Fig. 4 are responsible for dynamic compensation and steady state performance respectively and are discussed in Section IV-B and Section IV-C.

1) Observer Gain in Frequency Domain: Process-model mismatch and disturbances may be described by additional terms $\mathbf{d}_1(t) \in \mathbb{R}^r$ and $\mathbf{d}_2(t) \in \mathbb{R}^n$ as follows:

$$\begin{aligned}\dot{\mathbf{x}}(t) &= \mathbf{A}\mathbf{x}(t) + \mathbf{B}\mathbf{u}(t) + \mathbf{d}_1(t) \\ \mathbf{y}(t) &= \mathbf{C}\mathbf{x}(t) + \mathbf{D}\mathbf{u}(t) + \mathbf{d}_2(t)\end{aligned} \tag{19}$$

Subtracting $\dot{\tilde{\mathbf{x}}}(t)$ in (18) from $\dot{\mathbf{x}}(t)$ in (19), the equation for the residual $\mathbf{r}(t)$ can be derived as follows: [8]

$$\begin{aligned}\dot{\mathbf{e}}(t) &= (\mathbf{A} - \mathbf{K}\mathbf{C})\mathbf{e}(t) + \mathbf{d}_1(t) - \mathbf{K}\mathbf{d}_2(t) \\ \mathbf{r}(t) &= \mathbf{C}\mathbf{e}(t) + \mathbf{d}_2(t)\end{aligned} \tag{20}$$

where

$$\dot{\mathbf{e}}(t) = \dot{\mathbf{x}}(t) - \dot{\tilde{\mathbf{x}}}(t) \tag{21}$$

The Laplace transform of (20) is thus

$$\begin{aligned}\mathbf{r}(s) &= \mathbf{C}(s\mathbf{I} - \mathbf{A} + \mathbf{K}\mathbf{C})^{-1}\mathbf{d}_1(s) \\ &\quad + (\mathbf{I} - \mathbf{K}\mathbf{C}(s\mathbf{I} - \mathbf{A} + \mathbf{K}\mathbf{C})^{-1})\mathbf{d}_2(s)\end{aligned} \tag{22}$$

Subsequently, the effects of process-model mismatch and disturbances can be minimised using the following performance indices:

$$J_1(\mathbf{K}) = \left\| \mathbf{C}(s\mathbf{I} - \mathbf{A} + \mathbf{KC})^{-1} \right\|_\infty \tag{23}$$
$$J_2(\mathbf{K}) = \left\| \mathbf{I} - \mathbf{C}(s\mathbf{I} - \mathbf{A} + \mathbf{KC})^{-1}\mathbf{K} \right\|_\infty \tag{24}$$

where $\|.\|_\infty$ denotes L_∞ norm, also known as infinity norm. By minimising $J_1(\mathbf{K})$ and $J_2(\mathbf{K})$, the maximums of the largest singular values of $\mathbf{C}(s\mathbf{I} - \mathbf{A} + \mathbf{KC})^{-1}$ and $\mathbf{I} - \mathbf{KC}(s\mathbf{I} - \mathbf{A} + \mathbf{KC})^{-1}$, which correspond to the peak gains of the frequency response, are minimised. Hence, the effects of process-model mismatch and disturbances can be minimised.

If any information about the distrurbances or process-model mismatch is given, the vectors $\mathbf{d}_1(t)$ and $\mathbf{d}_2(t)$ may be reconstructed to approximate the effect of the disturbances and process-model mismatch as:

$$\begin{aligned} \mathbf{d}_1(t) &= \Delta\mathbf{A}\mathbf{x}(t) + \Delta\mathbf{B}\mathbf{u}(t) + \mathbf{E}_1\tilde{\mathbf{d}}_1(t) \\ \mathbf{d}_2(t) &= \Delta\mathbf{C}\mathbf{x}(t) + \Delta\mathbf{D}\mathbf{u}(t) + \mathbf{E}_2\tilde{\mathbf{d}}_2(t) \end{aligned} \tag{25}$$

where $\mathbf{E}_1$ and $\mathbf{E}_2$ are the disturbance distribution matrices and $\tilde{\mathbf{d}}_1(t)$ and $\tilde{\mathbf{d}}_2(t)$ are the disturbance vectors. $\Delta\mathbf{A}$, $\Delta\mathbf{B}$, $\Delta\mathbf{C}$ and $\Delta\mathbf{D}$ are the modelling errors.

The system in (19) is assumed to be controllable and observable. $\mathbf{d}_1(t)$ and $\mathbf{d}_2(t)$ are assumed to be bounded and not known. However, if some bounds on these signals can be estimated then good stability robustness may be incorporated in the design by adding these as constraints to the minimisation problems of the performance indices (23) and (24) or using H-infinity control design technique. However, this approach is not pursued here but good robustness is achieved by carefully tuning the controller and testing the controller against different disturbances and operating conditions. As a result, the effects of disturbances and modelling errors may be minimised even further resulting in improved robustness.

The problem now is to find $\mathbf{K}$ such that $J_1(\mathbf{K})$ and $J_2(\mathbf{K})$ are minimised. However, it is likely that $\mathbf{K}$ causes instability. This can be prevented by parameterising $\mathbf{K}$ via the eigenstructure assignment method summarised here.

2) Parameterisation via Eigenstructure Assignment Method: When conducting an optimisation to minimise $J_1(\mathbf{K})$ and $J_2(\mathbf{K})$ in (23) and (24), it is important to ensure that the stability of the observer is always guaranteed, assuming that no disturbance or fault is present, and this leads to more complex constrained optimisation problem. To guarantee the stability condition, Chen and Patton [8] suggest the use of the eigenstructure assignment method which parameterises $\mathbf{K}$. The method has an advantage of allowing the eigenvalues in predefined regions and is summarised as follows: First it is assumed that the eigenvalues are always real for the sake of brevity. Since the observer design problem is the "dual problem" of the controller design, $\mathbf{v}_i$ is the i_{th} eigenvector of $\mathbf{A}^T - \mathbf{C}^T\mathbf{K}^T$ corresponding to the i_{th} eigenvalue λ_i as follows:

$$(\mathbf{A}^T - \mathbf{C}^T\mathbf{K}^T)\mathbf{v}_i = \lambda_i \mathbf{v}_i \tag{26}$$
$$\mathbf{v}_i = -(\lambda_i \mathbf{I} - \mathbf{A}^T)^{-1}\mathbf{C}^T\mathbf{w}_i \tag{27}$$

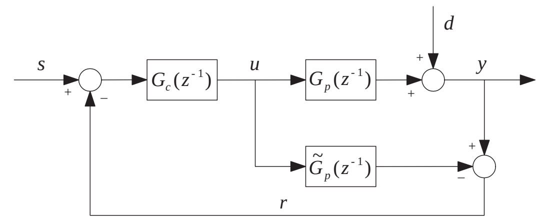

Fig. 5. Generic IMC Design

where $\mathbf{w}_i = \mathbf{K}^T\mathbf{v}_i$. There are now two design parameters $\mathbf{w}_i$ and λ_i instead of one design parameter $\mathbf{K}$. These design parameters still do not guarantee the stability of the observer.

The eigenvalue λ_i, one of the design parameters, is generally not required to be placed at a specific point in the s or z-planes but rather in a predefined region to satisfy the stability condition. This in turn provides more relaxed design freedom as follows:

$$\lambda_i \in [L_i, U_i] \tag{28}$$

where L_i and U_i $(i = 1, \dots n)$ respectively denote the upper and lower bounds. By defining an equation for the eigenvalue as

$$\lambda_i = L_i + (U_i - L_i sin^2(z_i)) \tag{29}$$

$z_i \in \mathbb{R}$ $(i = 1, \dots, n)$ becomes a design parameter instead of λ_i. Any z_i subsequently guarantees the stability condition.

Finally, the two design parameter vectors $\mathbf{W}$ and $\mathbf{Z}$ have been defined and the performance indices in (23) and (24) can be rewritten as follows:

$$J_1(\mathbf{W}, \mathbf{Z}) = \left\| \mathbf{C}(s\mathbf{I} - \mathbf{A} + \mathbf{KC})^{-1} \right\|_\infty \tag{30}$$
$$J_2(\mathbf{W}, \mathbf{Z}) = \left\| \mathbf{I} - \mathbf{KC}(s\mathbf{I} - \mathbf{A} + \mathbf{KC})^{-1}) \right\|_\infty \tag{31}$$

where

$$\mathbf{K} = [\mathbf{W}\mathbf{V}^{-1}]^T \tag{32}$$

Having redefined the multi-objective optimisation problem as finding $\mathbf{Z}$ and $\mathbf{W}$ from finding $\mathbf{K}$ only, the stability condition is always guaranteed.

Since, two performance indices (30) and (31) need to be minimised simultaneously, a multi-objective optimisation technique is required. The use of an evolutionary algorithm [9] is proposed here to solve the multi-objective optimisation problem. The controller design in this paper exploits a genetic algorithm. The algorithm is not presented here but readers are referred to [9] instead.

B. Dynamic Compensation

Bump test results can be used to approximate the dynamic response of the plant as follows:

$$h(z^{-1}) = \frac{1-\alpha}{1-\alpha z^{-1}} z^{-k} \tag{33}$$

where α is the time constant of the process. Recall that the proposed controller design benefits from not having to separate the spatial component from the dynamic component of the reference model. Although the bump tests provided the dynamic response of the model, the benefit claimed is still valid as the spatial component of the model is still unknown.

The generic IMC design illustrated in Fig. 5 usually designs $G_c(z^{-1})$ as the inverse of the reference model $\tilde{G}_p(z^{-1})$ so that if $\tilde{G}_p(z^{-1})$ is equal to $G_p(z^{-1})$, $y(t)$ is also equal to $s(t)$. However, $\tilde{G}_p(z^{-1})$ is usually non-invertible and should therefore be factorised into invertible and non-invertible components first as follows:

$$\tilde{G}_p(z^{-1}) = \tilde{G}_p^+(z^{-1})\tilde{G}_p^-(z^{-1}) \tag{34}$$

where the invertible component is given by

$$\tilde{G}_p^+(z^{-1}) = \frac{1-\alpha}{1-\alpha z^{-1}} \tag{35}$$

Subsequently, $G_c(z^{-1})$ can be designed as the inverse of $\tilde{G}_p^+(z^{-1})$. Furthermore, the effect of process-model mismatch can be minimised to improve robustness. Since mismatches generally occur at the high frequency region of the frequency response, a low-pass filter $G_f(z^{-1})$ is usually added to attenuate the effect of process-model mismatch as follows:

$$G_c(z^{-1}) = [\tilde{G}_p^+(z^{-1})]^{-1}G_f(z^{-1}) \tag{36}$$

where

$$G_f(z^{-1}) = \frac{1-\beta}{1-\beta z^{-1}} \tag{37}$$

Substituting (35) into (36), the equation for the controller is

$$G_c(z^{-1}) = \left(\frac{1-\alpha z^{-1}}{1-\alpha}\right)\left(\frac{1-\beta}{1-\beta z^{-1}}\right) \tag{38}$$

where $0 \leq \beta \leq 1$ is the low-pass filter bandwidth and can be tuned to reduce the effect of process-model mismatch.

The proposed controller design in Fig. 4 has a similar structure to Fig. 5. Therefore, $\mathbf{G}_c(z^{-1})$ in Fig. 4 is also given by (38) but as a diagonal transfer function matrix for the multi-variable process.

C. Steady State Performance

Optimal steady state performance can be achieved by minimising $\|\mathbf{y}(t)\|_2 = \|\tilde{\mathbf{y}}(t) + \mathbf{r}(t)\|_2$ where $\tilde{\mathbf{y}}(t)$ is given in (18) and $\|.\|_2$ denotes L_2 norm.

In the steady state, $\dot{\tilde{\mathbf{x}}}(t)$ in (18) is equal to zero and therefore the equation becomes

$$\tilde{\mathbf{x}}(t) = -\mathbf{A}^{-1}\mathbf{B}\mathbf{u}(t) - \mathbf{A}^{-1}\mathbf{K}\mathbf{r}(t) \tag{39}$$

Substituting (39) into the following

$$\tilde{\mathbf{y}}(t) = \mathbf{C}\tilde{\mathbf{x}}(t) + \mathbf{D}\mathbf{u}(t) \tag{40}$$

and assuming $\mathbf{D}$ is a zero matrix, the following can be derived:

$$\tilde{\mathbf{y}}(t) = -\mathbf{C}\mathbf{A}^{-1}\mathbf{B}\mathbf{u}(t) - \mathbf{C}\mathbf{A}^{-1}\mathbf{K}\mathbf{r}(t) \tag{41}$$

Since $\mathbf{y}(t) = \tilde{\mathbf{y}}(t) + \mathbf{r}(t)$

$$\mathbf{y}(t) = -\mathbf{C}\mathbf{A}^{-1}\mathbf{B}\mathbf{u}(t) + (\mathbf{I} - \mathbf{C}\mathbf{A}^{-1}\mathbf{K})r(t) \tag{42}$$

Hence, optimal steady state performance can be attained with

$$\mathbf{u}_{ss} = \arg\min_u \left\|-\mathbf{C}\mathbf{A}^{-1}\mathbf{B}\mathbf{u}(t) + (\mathbf{I} - \mathbf{C}\mathbf{A}^{-1}\mathbf{K})\mathbf{r}(t)\right\|_2 \tag{43}$$

where $\mathbf{u}(t)$ is subject to constraints, such as actuator saturation and bending constraints. The nonlinear element (NL) in Fig. 4 continuously produces the control action using (43). In order to solve the quadratic programming required for (43), " fmincon" function provided by the Optimization Toolbox™4.3 was utilised.

D. Computational Structure of the Controller

The proposed controller design can be summarised as follows (Fig. 4):

1) *Derivation of a reference model*: A reference model in state space form is derived.
2) *Design of an observer*, **K**: In order to find **K** to minimise the effects of process-model mismatch and disturbances, the genetic algorithm is exploited for the multi-objective optimisation problem. Moreover, the stability of the observer is guaranteed by the use of the eigenstructure assignment method summarised in Section IV.
3) *Dynamic compensation*: For dynamic compensation, the IMC design is employed (Section IV-B).
4) *Steady state performance*: Online optimisation is conducted to calculate optimal control action $\mathbf{u}_{ss}$ by continuously solving (43) (Section IV).

V. Implementation, Tuning, Validation, and Simulation

A. Model

1) Implementation and Parameter Tuning: The model has been implemented in Matlab/Simulink®. The model encompasses several hundred dynamic states. The model allows users to change the number of CD sections modelled, and the simulation results shown in Section V are for a 10 CD section model. This is considerably less than the number used in a typical CD control system. A realistic model requires around 250 CD sections to capture detailed dynamics and ill-conditioned nature of the process and the proposed model can be extended to include more sections. However, in common with many other process control design practices, a reduced order model is used here to capture the main dynamics and derive models for control design purposes. The model has been tuned using a set of typical real measurements which include operational and geometrical parameters such as process speed, temperature, heat transfer coefficients, and die geometry.

2) Validation: Although the model can predict other film properties, the main purpose of the model is to predict the film thickness (or basis weight (kg/m^2), which is linearly related to thickness). The validation experiments carried out have therefore mainly focused on the ability of the model to predict this property. The validation included mapping or comparing the film thicknesses that the model predicts at various locations such as die outlet and sideways draw outlet with real data.

Another validation method was to compare the model predictions with those from the empirical model described in (44). The empirical model has been derived from identification trials similar to those reported in [10] and [11].

$$\mathbf{y}_t = q^{-d}g(q^{-1})k_p\mathbf{G}\mathbf{u}_t \tag{44}$$

where $\mathbf{u}_t$ and $\mathbf{y}_t$ respectively represent actuator set-points and the thickness profile. $\mathbf{G}$ is the interaction matrix representing the spatial response, which for this process gives each actuator the response of a Gaussian curve, k_p is the process gain, d is the integer process delay, and $g(q^{-1})$ represents the discrete form of a first order model [10]. $\mathbf{G}$ has one row for each output measurement and one column for each actuator.

The results showed that the deviation between the prediction of the nonlinear model and the measurement data and the deviation between the prediction of the nonlinear model and the empirical model both remained within a 5% margin.

Finally, to compensate for locations where real data are not available, a number of open-loop step response tests at various locations were carried out, and the results were validated against the process by the expert operators.

B. *Controller*

A number of simulations have been conducted to demonstrate how the controller performs, and three of these simulations are depicted in Figs. 6, 7, and 8. These simulations have been conducted not only for the proposed controller but also for the industrial controller reported in [10] and another model-based controller reported in [3] for comparison purposes. Figs. 6, 7 and 8 show the steady state CD thickness profile measured by the scanning gauge and the corresponding actuator set-points. Red plots are for the "Proposed" controller; blue plots are for the "Industrial" controller; and black plots are for the one reported in [3] and labelled as "IMC". It was assumed that the film was divided into 10 lanes (Section III). To simulate what happens in real-life, the edges – the first and last lanes – were not controlled and left open-loop instead. Therefore, the figures do not show the first and last lanes. The y-axes represent thickness in percentage deviation from the mean, and the x-axes denote the CD position.

The existing controllers reported in [3] and [10] employ the model given in (44) as the reference model. However, for the proposed controller design, a linear model is directly identified from the nonlinear model. The model in (44) on the other hand has been identified directly from a real plant as opposed to the nonlinear model. Although the model has been developed to simulate the plant, a mismatch between the plant and the model still exists. Therefore, the existing controllers would experience larger model-plant mismatch than the proposed controller making the comparison unfair. As a result, the reference model for all controllers has been identified using the model in (44). The resulting model is a state space model with $\mathbf{A} \in \mathbb{R}^{r\times r}$, $\mathbf{B} \in \mathbb{R}^{r\times n}$, $\mathbf{C} \in \mathbb{R}^{n\times r}$, and $\mathbf{D} \in \mathbb{R}^{n\times n}$, where n and r are respectively 10 and 14. Further details of this model can be found in [7]

If the reference model is identified from the nonlinear model, improved performance of the proposed controller can be expected. It is also important to point out that the industrial controller has been tuned to work optimally with the plant as opposed to the nonlinear model, which implies that improved performance of the industrial controller can also be expected with improved tuning parameters. Furthermore, the IMC controller reported in [3] has a number of different versions which are not presented here.

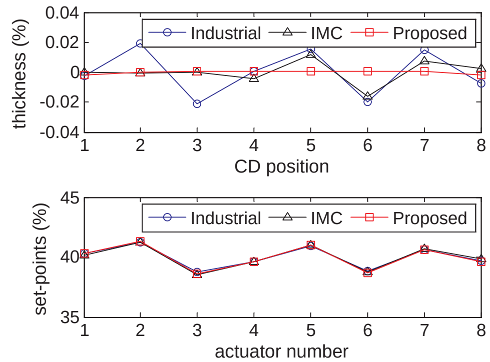

Fig. 6. Simulation 1: Steady state CD thickness profile under normal operational conditions

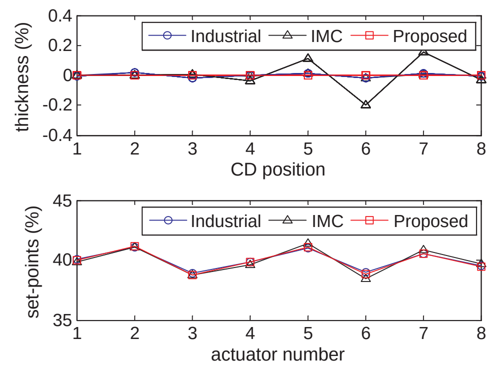

Fig. 7. Simulation 2: Steady state CD thickness profile with fast-roll speed variation from $t = 0s$; y-axis of upper plot has a different range from those in Fig. 6 and Fig. 8

Subsequently, all the controllers have been tuned and applied to the nonlinear model and the simulation results are summarised as follows: In Simulation 1, set point tracking is tested. The proposed controller achieves a noticeable improvement over the existing controllers under normal operating conditions as shown in Fig. 6. Although no disturbances are present, the set-points are not flat because model-plant mismatch exists under normal operating conditions. As the proposed controller is designed to minimise the effect of model mismatch, it demonstrates better robustness.

In Simulation 2, persistent variation in fast-roll speed is introduced. The speed varies randomly within $\pm 10\%$ of the desired speed. The proposed controller achieves a noticeable improvement over the IMC controller and a slight improvement over the industrial controller.

A polymer melt is fed into the die at a certain mass flow rate (Section II). In Simulation 3, mass flow rate starts to vary suddenly from $3000s$ in contrast to Simulation 2, where the variation occurs from $0s$. The purpose of this simulation is to see how the controller responds to a disturbance appearing suddenly. Mass flow rate varies randomly within $\pm 10\%$ of the desired rate. Fig. 8 shows that the proposed controller achieves a noticeable improvement over the industrial controller but has a similar performance to the IMC controller.

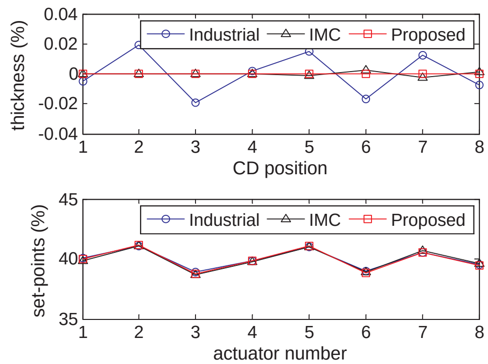

Fig. 8. Simulation 3: Steady state CD thickness profile with mass flow variation from $t = 3000s$

TABLE I
COMPARISON OF CONTROLLERS

	σ_P^2 (%)	σ_I^2 (%)	σ_M^2 (%)	τ_P (s)	τ_I (s)	τ_M (s)
S1	$1.1e^{-6}$	$243.6e^{-6}$	$67.6e^{-6}$	0.11	0.00	0.05
S2	$0.18e^{-6}$	$212.38e^{-6}$	$11203.70e^{-6}$	0.11	0.00	0.05
S3	$0.003e^{-6}$	$215.487e^{-6}$	$0.024e^{-6}$	0.11	0.00	0.05

e denotes $\times 10$

Figs. 6, 7 and 8 demonstrate that the steady state actuator set-points for the proposed controller are close to those of the industrial controller for all the simulations. Despite this, the thickness profiles look quite different when they are expected to be the same. This is because when the process reaches steady state, the online optimisation used for solving (43) hardly stops fine-tuning the proposed controller, thereby improving the thickness profiles even further.

To compare the computation load of the controllers, the time τ (s) taken by each controller per each call on a AMD™Phenom X4 955 GHz machine is given in Table I. P, I, and M denote "Proposed", "Industrial", and "IMC" controllers, and S "Simulation". Moreover, the variance σ^2 of the thickness are also tabulated and this clearly demonstrates the superior steady-state performance of the proposed controller.

VI. Conclusion

Nonlinear models of the plastic film manufacturing web process are still rare as these models are regarded difficult and time consuming to build. Nonetheless, this paper introduces such a model, taking account the characteristics of each unit of the process. The model can be utilised in many ways including testing different operational scenarios for tuning the process as well as training the operators. Moreover, it allows control algorithms to be developed and tested.

A new model-based CD controller is also proposed and compared with existing controllers. The simulation results demonstrate improved performance for both steady-state and dynamic conditions. The improvements are mainly due to the observer whose gain is designed to minimise the effects of process-model mis-match and disturbances.

Acknowledgment

The authors would like to acknowledge financial support from DuPont Teijin Films UK Ltd, UK EPSRC Industrial CASE Award, and UK EPSRC Platform Grant (GR/R04683/01). The authors would also like to thank Dr Jonas Balderud and DuPont Teijin Films UK Ltd for their contributions to the modelling section of this work.

References

[1] J. G. VanAntwerp, A. P. Featherstone, R. D. Braatz, and B. A. Ogunnaike, "Cross-directional control of sheet and film processes," *Automatica*, vol. 43, pp. 191–211, 2007.

[2] A. Featherstone, J. VanAntwerp, and R. Braatz, *Identification and control of sheet and film processes*, ser. Advances in Industrial Control. London: Springer, 2000.

[3] W. P. Heath and A. G. Wills, "Design of cross-directional controllers with optimal steady state performance," Centre for Integrated Dynamics And Control (CIDAC), University of Newcastle, NSW, 2380, Australia, Tech. Rep., 2002.

[4] T. Kanai and G. Campbell, *Film Processing*, W. Baker, Ed. Hanser Gardner Publications, 1999.

[5] S. Sutera and R. Skalak, "The history of poiseuille's law," *Annual Review of Fluid Mechanics*, vol. 25, pp. 1–19, 1993.

[6] S. Hur, "Monitoring and control of the cross directional plastic film," University of Strathclyde," Industrial Control Centre Report, 2008.

[7] ——, "A model-based cross directional control of a plastic film making process," University of Strathclyde," Industrial Control Centre Report, 2009.

[8] J. Chen and R. J. Patton, *Robust model-based fault diagnosis for dynamic systems*, K.-Y. Cai, Ed. Kluwer Academic Publishers, 1999.

[9] A. Konak, D. W. Coit, and A. E. Smith, "Multi-objective optimization using genetic algorithms: A tutorial," *Reliability Engineering and System Safety*, vol. 91, pp. 992–1007, 2006.

[10] A. Taylor and S. Duncan, "Actuator mapping and stability in real-life cross-directional control systems," in *Control Systems 2006, Tampere, Finland*, 2006, pp. 191–196.

[11] D. Gorinevsky and C. Gheorghe, "Identification tool for cross-directional processes," *IEEE Transactions on Control Systems Technology*, vol. 11(5), pp. 629–640, 2003.

Sung-ho Hur received the B.Eng. degree in Electronics and Electrical Engineering from University of Glasgow, U.K, in 2004 and the M.Sc. degree with Distinction and Ph.D. degree in Electronic and Electrical Engineering from University of Strathclyde, U.K, in 2005 and 2010. He is currently a Research Fellow with the Department of Electronic and Electrical Engineering at University of Strathclyde, U.K. His research interests are in the areas of process control, process modelling, and condition monitoring.

Reza Katebi is a Reader in control engineering at the Industrial Control Center, Department of Electronic and Electrical Engineering, University of Strathclyde. Reza's current research interests are focused on the modeling and control of complex and networked control systems with applications to Marine, Automotive, and Wastewater systems. He has authored/coauthored five books, more than 150 publications and served as IPC of a number of IEEE and IFAC conferences. He is also an associate editor of Automatica, on editorial board of Journal of Marine Science and Technology, Springer Japan and application editor for Journal of Adaptive Control and Signal Processing. Reza is the holder of Denny Medal (JMET), 2006 , of The Institute of Marine Engineering, Science, and Technology.

Andrew Taylor received the B.Sc. degree in Statistics in 1988 from the University of Aberdeen and the D.Phil degree from the University of Oxford in 2004. He is a Senior Process Engineer with DuPont Teijin Films UK Ltd and has previously been employed by the University of Newcastle Upon Tyne and Imperial Chemical Industries PLC. His current research interests are in the monitoring and control of industrial processes and cross-directional control of web forming processes. He is a Fellow of the Royal Statistical Society.